

Supplementary information

Understanding the partitioning behavior of single-walled carbon nanotubes using an aqueous two-phase extraction system composed of non-ionic surfactant and polymer

Pranjala Tiwari^{1,*}, Błażej Podleśny¹, Maciej Krzywiecki²,
Karolina Z. Milowska^{3,4,5}, Dawid Janas^{1,*}

¹ *Department of Chemistry, Silesian University of Technology, B. Krzywoustego 4, 44-100, Gliwice, Poland*

² *Institute of Physics-CSE, Silesian University of Technology, Konarskiego 22B, 44-100 Gliwice, Poland*

³ *CIC nanoGUNE, 20018 Donostia-San Sebastián, Spain*

⁴ *Ikerbasque, Basque Foundation for Science, 48013 Bilbao, Spain*

⁵ *TCM Group, Cavendish Laboratory, University of Cambridge, Cambridge CB3 0HE, United Kingdom*

*Corresponding authors: Pranjala.Tiwari@polsl.pl (Pranjala Tiwari), Dawid.Janas@polsl.pl (Dawid Janas)

Table of Contents

1. Experimental.....	3
1.1. Chemical compounds	3
1.2. Preparation of SWCNT dispersions.....	3
1.3. ATPE protocol.....	4
1.4. Binodal curves	4
1.5. Density and volume determination	5
1.6. Optical characterization	7
1.7. XPS characterization	7
1.8. Modelling	10
2. Results and discussion	13
2.1 Analysis of the biphasic systems	13
2.2 Selection of appropriate SWCNT dispersions for partitioning	15
2.3 Selection of appropriate surfactant for SWCNT differentiation	17
2.4 Analysis of purification process	18
2.4.1. Redistribution of SWCNTs because of addition of SDS of various concentrations	18
2.4.2. Processing of different SWCNT raw material	18
2.4.3. Application of SDBS as partitioning modulator	19
2.4.4. Quantification of composition of isolated SWCNT fractions	19
2.4.5. Modeling of SWCNT-surfactant interactions	20
2.5 Insights into the separation mechanism	22
2.5.1. Change in SWCNT density upon absorption of surfactant molecules on the surface.....	22
3. References	23

1. Experimental

1.1. Chemical compounds

Dextran (DEX, MW ca. 70,000 Da), sodium cholate hydrate (SC), sodium deoxycholate (DOC), Pluronic L-35 (PL-35), sodium dodecyl sulfate (SDS), sodium dodecylbenzene sulfonate (SDBS), Brij 35 (MW, ca. 1,198 Da), and DNA (from fish sperm) were obtained from Sigma-Aldrich. Poly(ethylene glycol) (PEG, MW ca. 2,000 Da) was purchased from Alfa Aesar. (6,5)-enriched SWCNTs prepared via CoMoCAT synthesis and unsorted HiPco SWCNTs purchased from CHASM Advanced Materials were used in the sorting process.

1.2. Preparation of SWCNT dispersions

All dispersions (SWCNTs in aqueous solutions of DOC, SDS, DNA, and Brij) were prepared using the same protocol, in which 2 wt.% of the respective surfactant was first dissolved in 40 mL of water. Next, SWCNT powder was added to a stock solution, where the total amount of SWCNTs was maintained at 1 mg/mL in water. The mixture was homogenized using an ultrasound tip sonicator (Hielscher UP200St) for 200 min at 30 W constant power over ice. The temperature of the ice-water bath did not exceed 1°C (Figure S1).



Figure S1 Ice-cooled setup used for sonication of SWCNTs.

The selection of low sonication power ensured that the temperature of the sample remained low. After the sonication process was completed, we unmounted the vessel used for sonication from the setup, which was cold, indicating that the samples were not subjected to overheating.

The obtained dispersion was then centrifuged (Eppendorf Centrifuge 5430 R) for 180 min at 11,000 rpm (corresponding to $15,314\times$ g RCF). Finally, the top 80% of the supernatant was collected and used for further experiments.

1.3. ATPE protocol

Stock solutions of polymers PEG, DEX, PL-35 (concentrations of 25 wt%, 20 wt%, and 25 wt%, respectively) and various modulators (2% SC, 5% DOC, 2-10% SDS and 2-10% SDBS concentration) were prepared using a vortex mixer and centrifuge and utilized for ATPE experiments. ATPE separation was conducted by combining PL-35/PEG and DEX (1:1, v/v), where the total volume of the system was 4 mL and the resulting concentrations of the top and bottom phase components were 12.5% and 10%, respectively. Next, 100 μ L of SWCNT dispersion ((6,5)-enriched or unsorted HiPco) was added into the sample. Then, various modulators (aqueous dispersions of SC, DOC, SDS, and SDBS) were added in a wide range of concentrations, after which the suspensions were vortexed and centrifuged to facilitate phase separation. Note, the total volume of ATPE system for each test sample increased after addition of the external modulator (e.g. SDS). All ATPE experiments were carried out at room temperature (20°C).

1.4. Binodal curves

Appropriate quantities of PL-35, PEG, and DEX were weighed and dissolved in water to various concentrations in order to create binodal curves. PL-35/DEX and PEG/DEX binodal curves were constructed using the cloud-point titration method ¹. In the first step, aqueous

solutions of PL-35 or PEG were added dropwise to DEX, under constant stirring, until a cloudy point appeared. After that, the system was diluted to establish conditions equivalent to monophasic regime. Subsequently, more PL-35 or PEG was added until turbidity was observed again. In the second step, the reverse procedure was adopted, wherein the initial solution contained PL-35 or PEG, to which DEX was added gradually until the cloud point was reached and removed by dilution. Finally, the overall percentage of added DEX and PL-35/PEG was calculated at each cloud point to obtain a binodal curve. All titration experiments were carried out at room temperature (20°C).

1.5. Density and volume determination

Density was determined by pycnometry. All stock solutions were examined under the same conditions. First, a calibrated pycnometer was incubated at room temperature (20°C) using the examined stock solutions to equilibrate the temperature. Then, ca. 2 mL of the solution was pipetted into the pycnometer, after which the outlet was carefully closed with a stopper. The surplus droplets were removed, the measurement apparatus was placed on an analytical balance, and the weight was recorded. The vessel was repeatedly washed with deionized water and acetone between each measurement. Once the pycnometer was dried, another measurement was recorded only after the temperature of the cleaned glass stabilized. To estimate the volumes of the top/bottom phases, the samples were prepared as described by ATPE protocol using a custom-made setup containing small, graduated cylinder made from glass (0.1 mL graduation) as the vessel. After combining all ATPE components and SWCNTs in the cylinder, the sample was homogenized by vortex mixing. Next, the cylinder was placed in a centrifuge tube, wherein the entire ATPE partitioning system was centrifuged. Finally, upon reaching phase separation, the cylinder was removed from the centrifuge tube, placed on a flat surface, and the phase volumes were recorded with the naked eye. Figure S2 illustrates the devised approach.

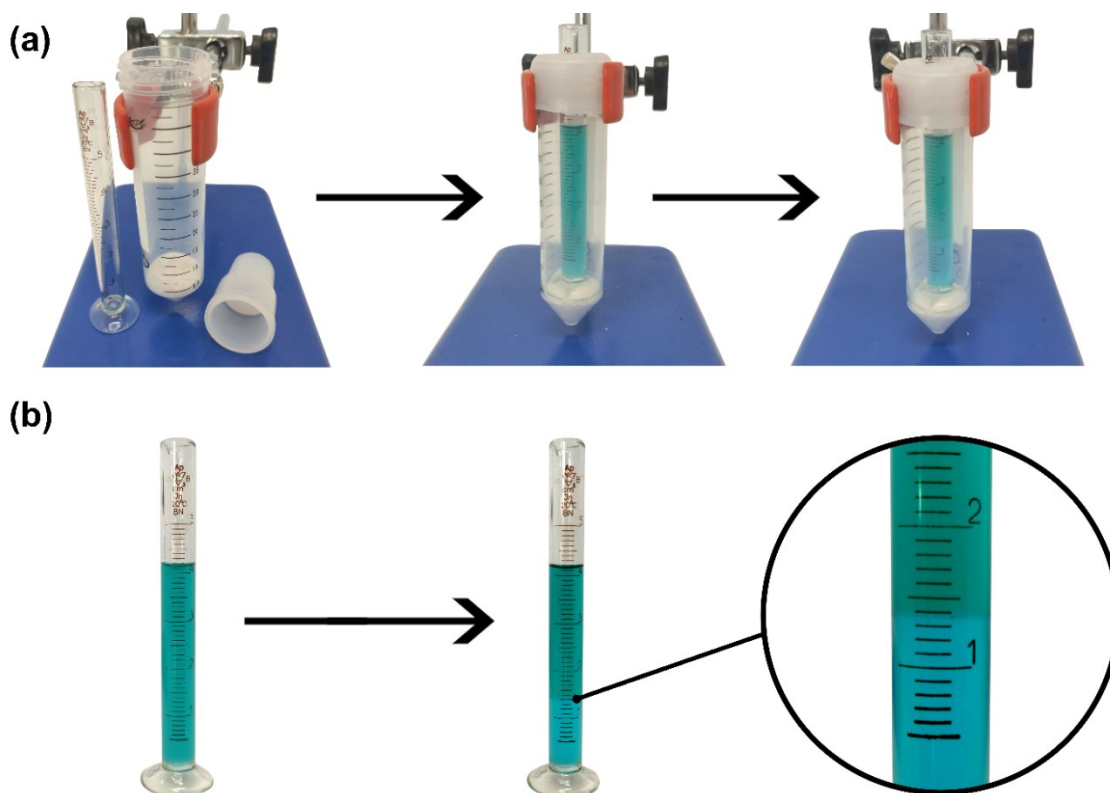


Figure S2 (a) Step 1: Elements of the developed setup for volume determination are combined, and ATPE components, including purified material, are injected. Step 2: The material occupying the cylinder is subjected to centrifugation *in situ* to facilitate phase separation. (b) Optical images of the ATPE components depicting the analyte before and after centrifugation. The provided magnification highlights that volume measurement using this technique is precise and straightforward.

In the presented case, 2 mL of DEX (20%) was combined with 2 mL of PL-35 (25%), mimicking the conditions used for SWCNT separation. Additionally, 33.3 μ L of saturated aqueous solutions of methylene blue, malachite green, and phenol red were injected into the biphasic system to visualize phase separation in the photographs. These dyes were not engaged while analyzing the biphasic systems.

Initial validation of this new approach for measuring density changes in ATPE showed that the recorded error does not exceed 0.022%. For these first trials, the density of DEX (20%) solution was measured eight times, giving the following values: 1.0802 g/mL, 1.0802 g/mL, 1.0807 g/mL, 1.0803 g/mL, 1.0806 g/mL, 1.0808 g/mL, 1.0804 g/mL, and 1.0808 g/mL. This translates to 1.0805 ± 0.0002 g/mL, giving the error level on the order of 0.022%. The uncertainty was on the same level when other analytes were examined.

1.6. Optical characterization

Optical characterization of the starting material (parent sample), as well as separated top and bottom phase samples, was carried out using a U-2910 Hitachi spectrophotometer over a wavelength range of 400-1100 nm. In addition, UV-Vis-NIR absorption spectra in the wavelength range of 400-1250 nm were obtained using a Perkin Elmer (Lambda 1050) spectrophotometer for specific samples. Where indicated, spectral data was resolved into components corresponding to particular chiralities using PTF Fit application ². Background, which seemed to follow the lineshape postulated by Nair et al. ³, was subtracted to improve the quantification precision.

1.7. XPS characterization

In order to investigate whether homogenization by sonication introduced defects in the material, it was characterized by X-ray photoelectron spectroscopy (XPS). The results are given in Figs. S3 and S4.

XPS measurements were performed in an ultra-high vacuum experimental setup (base pressure $9.5 \cdot 10^{-9}$ Pa) with a PREVAC EA15 hemispherical electron energy analyzer equipped with the 2D-MCP detector. A monochromated X-ray source (PREVAC dual-anode XR-40B source, RMC50 monochromator; Al-K α excitation line with energy 1486.60 eV) was utilized for sample excitation. Pass energy was set to 200 eV (with a scanning step of 0.8 eV) for survey spectra collection and to 100 eV (with a scanning step of 0.06 eV) for high-resolution energy regions. In order to optimize energy resolution and signal intensity, the spectra were acquired with a normal take-off angle and the curved analyzer exit slit. The binding energy scale of the analyzer was calibrated with respect to the Au 4f_{7/2} (84.0 eV) region of the gold-covered sample being kept at the same sample stage ⁴. Post-measurement processing of data was done using CASA XPS® software (version 2.3.25) with the

application of embedded algorithms. The components were fitted with the sum of Gauss (30%) and Lorentz (70%) functions and the Shirley function as a representation of the background signal.

Survey spectra (Figure S3) indicated that the parent material used for SWCNT sorting was of high quality as it contained only carbon and a negligible amount of oxygen. The presence of oxygen stemmed from the presence of various adventitious adsorbates that commonly contaminate nanocarbon material ⁵. No signs of residual catalyst were discerned. Furthermore, the samples dispersed in aqueous solutions of SC, besides oxygen and carbon, also included sodium atoms, which were contributed by the surfactant molecules. Overall, no significant differences were observed between the top two survey spectra of SWCNTs sonicated for 20 and 200 minutes.

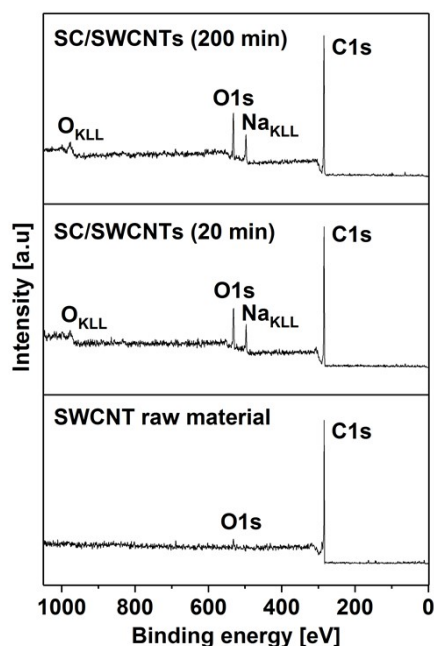


Figure S3 Survey spectra of SWCNT material used to prepare SWCNT dispersions along with spectra of the same material dispersed with SC in water by means of sonication conducted for 20 min and 200 min.

The recorded C1s and O1s peaks were deconvoluted to gain more insight into the possible influence of sonication (Figure S4). The analysis confirmed that the raw SWCNT powder

was highly crystalline as the signal from carbon atoms of sp^2 hybridization dominated the spectrum (Figure S4a). A small amount of previously mentioned oxygen-containing species was confirmed in the O1s spectrum (Figure S4b).

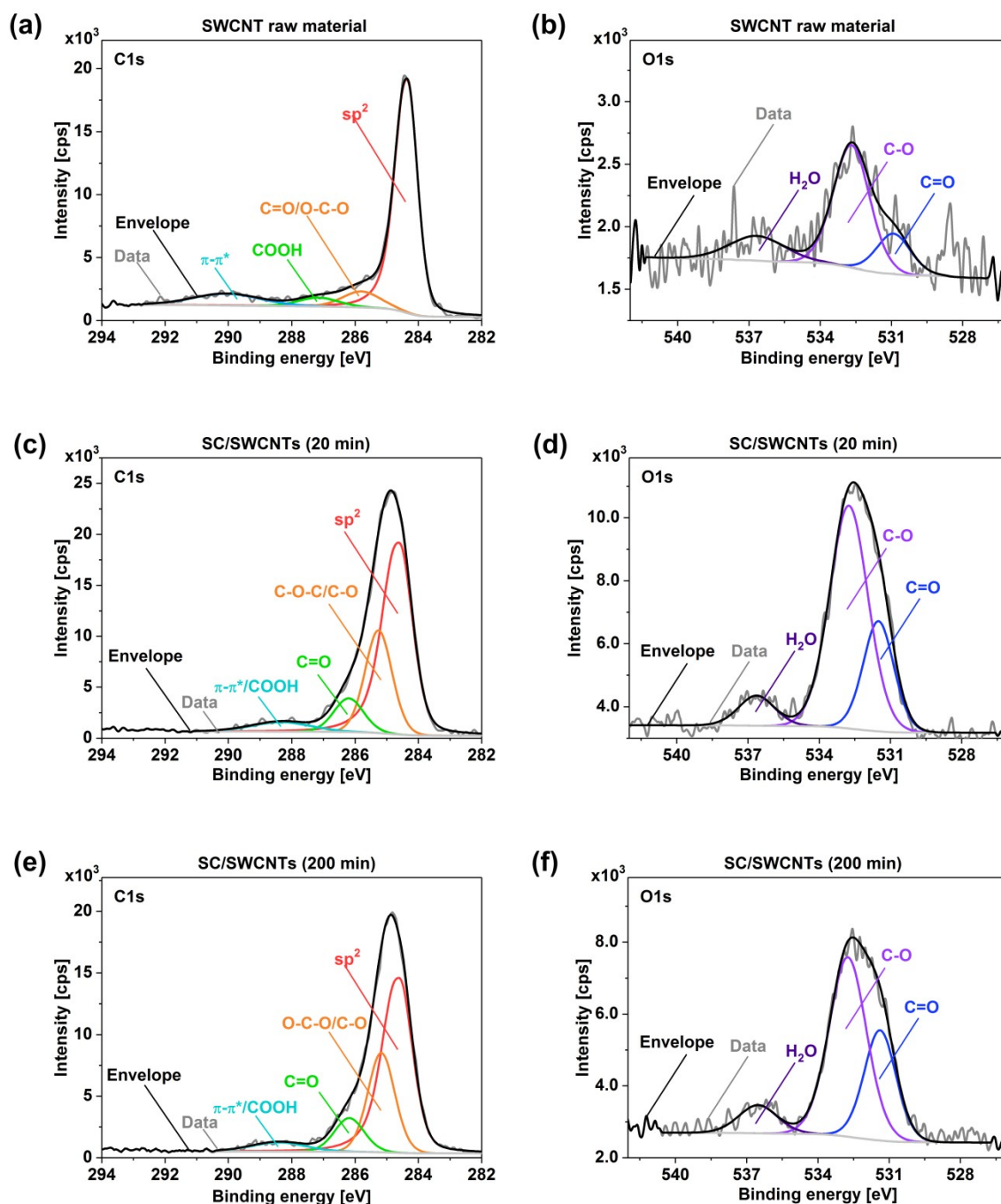


Figure S4 Deconvoluted (a,c,e) C1s and (b,d,f) O1s spectra of raw SWCNTs along with data registered for samples homogenized in aqueous SC solution by means of sonication conducted for 20 min and 200 min.

Most importantly, the characterization by XPS validated that the low-power sonication did not deteriorate the SWCNTs, which often damages the material when conducted for a prolonged time or under high amplitude conditions ⁶⁻⁸. The spectra provided in Figure S4cd and S4cd were indistinguishable even though the latter set of data came from samples obtained in water after 200 minutes of homogenization instead of 20 minutes. If the approach was destructive, it should be possible to note gradual functionalization of the material.

It is crucial to keep in mind that the relatively high intensity of oxygen-containing functional groups in the discussed spectra came from the presence of SC on the surface of SWCNTs. Each of the surfactant molecules contains three hydroxyl and one carbonyl group, which elevated the intensity of these bands. Besides that, SC is mainly made of sp³-hybridized carbon atoms, which increases the apparent level of disorder even further.

1.8. Modelling

Aqueous SDS and SDBS adsorption onto (6,5) SWCNT were investigated using a full periodic table bonded valence forcefield - an Universal Force Field (UFF) potential ⁹, as implemented in QuantumATK ^{10,11}. Energy contributions to the UFF potential were represented by simple functions based on bond lengths, bond angles, torsion angles, inversion angles, and inter-atomic distances. The electrostatic interactions were calculated using smooth-particle-mesh-Ewald (SPME) solver ¹². The cutoff used for calculating the real-space interactions was set to 7.5 Å, while the relative accuracy of SPME summation to 0.0001. Atomic partial charges on each atom were assigned using QEq charge equilibration method ¹³. Dispersive interactions were included in the form of Lennard-Jones potential ¹⁴⁻¹⁶ with 10 Å cutoff and 2 Å smoothing length.

We constructed six models of (6,5) SWCNT covered with varying numbers of surfactant molecules in water. Each simulation box contained one unit of (6,5) SWCNT surrounded by

symmetrically distributed SDS or SDBS molecules in layers around SWCNT cross-section. Surfactant molecules were placed perpendicular to SWCNT symmetry axis (*Z*-axis), forming one surfactant layer with three molecules along SWCNT symmetry axis for the low-concentration models and eight layers per eleven surfactant molecules, which covered SWCNT surface completely for high concentration models. In order to consider medium surfactant concentration, four surfactant layers (two from each side of the supercell along the *Z*-direction) per eleven molecules were removed from supercells containing 88 surfactants. This left only half of SWCNT surface covered with surfactants and the other half fully exposed to contact with water. Simulations boxes with dimensions of 8 nm, 8 nm, and 4 nm along *X*, *Y*, and *Z* directions were filled with 6160 water molecules using Packmol¹⁷ implemented in QuantumATK¹¹. 3D periodic boundary conditions were applied in all calculations, but the number of water molecules was sufficient to avoid direct interactions between SWCNT-surfactant complex images.

Prior to conducting molecular dynamics (MD) simulations, all systems were briefly optimized (5000 steps) using LBFGS algorithm¹⁸. MD simulations were carried out in NVT ensemble employing a Berendsen thermostat¹⁹ at 300 K. Random initial velocities of all atoms were assigned according to the Maxwell-Boltzmann distribution. The relaxation time of the thermostat was set to 100 fs, and the simulations were carried out with a time-step of 0.01 fs over a time period of 0.5 ps (5,000 steps). These simulations were followed by 5 ps (50,000 steps) NPT simulations at 300 K and 1 bar employing Berendsen thermostat and barostat. The thermostat and barostat relaxation times were set to 100 fs and 500 fs, respectively. The time step was kept the same as for previous simulations. The Martyna-Tobias-Klein²⁰ barostat and thermostat were used for another 5 ps (50,000) NPT simulations, employing the same parameters.

To investigate the interactions between surfactants and SWCNT on longer timescales, the time-stamped force-bias Monte Carlo method ^{21,22} was implemented in the QunatumATK numerical package ¹¹ to all resulting systems. MC simulations were carried out over a time period of 132.78 ps (100,000 steps) at 300 K and 1 bar. During MC simulations, the maximum atom displacement was set to 0.05 Å, and the estimated compressibility of the system related to volume changes to pressure changes was set to 0.0001 bar⁻¹. For two systems containing 44 surfactant molecules, additional 1.3278 ns (1,000,000 steps) MC simulations were added to test the stability of surfactant orientation. RDF and density profiles were calculated using the data obtained during 80 ps and 800 ps after equilibration in short and extended MC simulations, respectively.

2. Results and discussion

2.1 Analysis of the biphasic systems

First, a comparative study was conducted of PEG and PL-35 using the phase diagrams of PL-35/DEX and PEG/DEX as reference (Figure S5a). PL-35 of a comparable molecular weight (ca. 1.9 kDa) was utilized as a substitute for the top phase (PEG with an average molecular weight of 2.0 kDa) to minimize the possible differences, which could affect the partitioning. Surprisingly, the binodal curves had an analogous lineshape despite the obvious differences between the chemical structures (Figure S6) and densities. The densities of both 25% stock solutions in water at room temperature (20°C) were determined as 1.043 and 1.034 g/mL, for PEG and PL-35, respectively. PEG density was slightly higher, which may partially stem from the small but noticeable difference in molecular weight (ca. 5%).

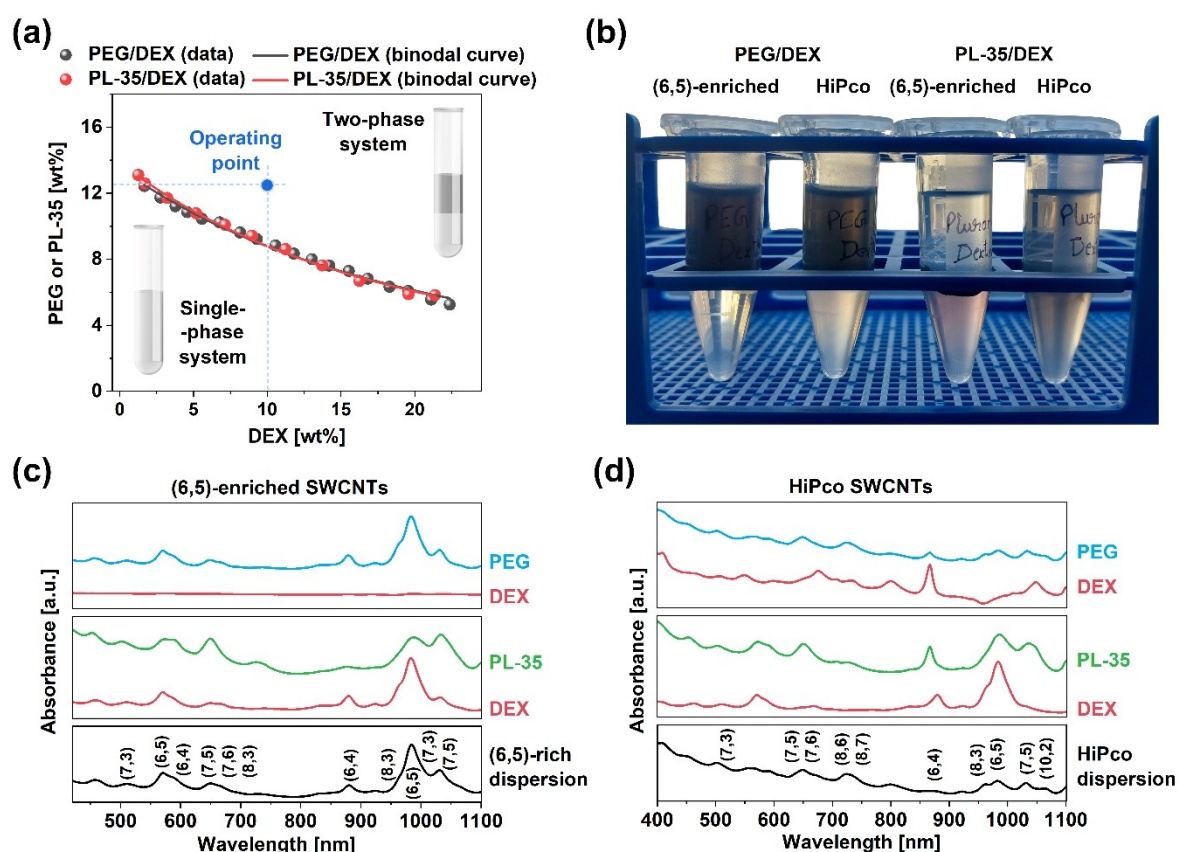


Figure S5 (a) Comparative analysis of PL-35/DEX and PEG/DEX biphasic systems, (b) Optical images of two types of SWCNT dispersions separated in PL-35/DEX and PEG/DEX systems. Absorption spectra of the separated phases are presented in panels (c) and (d) for (6,5)-enriched and HiPco SWCNTs, respectively.

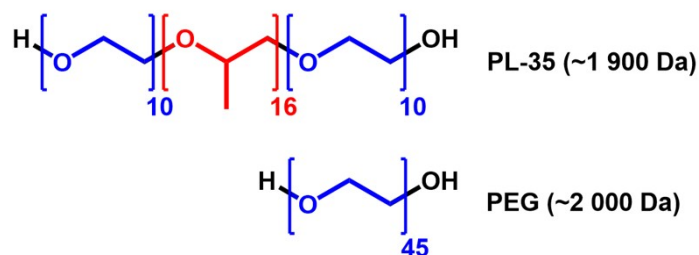


Figure S6 Structural differences between PL-35 and PEG. Hydrophilic and hydrophobic parts are colored in blue and red, respectively.

Next, concentrations of 12.5 wt% and 10.0 wt% were selected for the top and bottom phases, respectively, that formed the biphasic systems (Figure S5a). These biphasic systems were utilized to study their role in the separation of SWCNT mixtures. Equal amounts of (6,5)-enriched CoMoCAT SWCNT and HiPco SWCNT dispersions with 2% DOC were added to both PL-35/DEX and PEG/DEX systems, and the differences were recorded. Despite the similar parameters of PL-35 and PEG, as described above, a clear contrast between the studied separation media was observed (Figure S5b). The optical images showed that in PEG/DEX system, the majority of SWCNTs resided in the top phase, which was depicted by a dark black color. However, PL-35/DEX seemed to distribute SWCNTs between both phases, indicating a certain amount of selectivity. Unlike PEG, PL-35 is a surfactant, and surfactants, as previously highlighted, drive the ATPE method²³. Although PL-35 formed the top phase, the top phase component was also present in the bottom phase, according to the thermodynamics of biphasic systems²⁴. Hence, the presence of PL-35 in the bottom phase, even though a small amount, justified SWCNTs being observed by the naked eye in the bottom phase of PL-35/DEX system.

To gain a greater understanding of this contrast, the phases were separated into four samples and analyzed by absorption spectroscopy (Figures S5c,d). Spectroscopic results confirmed that PEG/DEX system had SWCNTs in the top phase regardless of type of raw material processed (the shape of the spectra from the top phases replicated parent dispersions).

Interestingly, in the case of HiPco SWCNTs, a small amount of SWCNTs was detected in the bottom phase with a relatively high abundance of (6,4) SWCNTs, typically present in negligible amounts²⁵. In contrast, the bottom phase of PEG/DEX system from the separation of (6,5)-enriched SWCNTs did not contain SWCNTs.

However, the application of PL-35/DEX system led to the distribution of SWCNTs between the top and the bottom phases, irrespective of SWCNT dispersion type. While the bottom phases were rich in small-diameter SWCNTs, such as (6,4), (8,3), and (6,5), the corresponding top phases also contained larger-diameter SWCNTs, such as (7,5). Furthermore, the top phases did not resemble parent dispersions. Therefore, the newly developed biphasic system exhibited a certain degree of selectivity, suggesting that the top-phase component (PL-35) played an active role in the separation process, possibly due to its amphiphilic character.

Previously, Lyu et al. reported that a change in the molecular weight of PEG mildly effected the differentiation course²⁶. They showed that the decrease in molecular weight increased the concentration of small-diameter SWCNTs, such as (6,5) and (8,3), in the top phase. However, it should be noted that the spectrum's shape was essentially unchanged, where the selectivity remained constant while the overall concentration of SWCNTs in the top phase increased. In our case, the difference in molecular weight between PEG and PL-35 was small, hence, it was more likely that the differences in the separation stemmed from the dissimilarity of the chemical nature of the phase-forming compounds. This hypothesis is further explored in section 2.3.

2.2 Selection of appropriate SWCNT dispersions for partitioning

It is essential to underline the importance of SWCNT dispersant selection. Similarly, as the addition of surfactant into ATPE system moves particular SWCNTs up and down, the type of surfactant attached to SWCNT side wall played a significant role. The partitioning was only

possible when SWCNTs were covered with a sufficient amount of DOC, which strongly forced SWCNTs to the bottom phase due to its hydrophilic character²³. Therefore, in the case of HiPco, a certain amount of SWCNTs was detected in the bottom phase, even in the absence of partitioning modulators or without the introduction of additional surfactant into the system. Attempts to incorporate other SWCNT dispersions in PL-35/DEX system were unsuccessful (Figure S7).

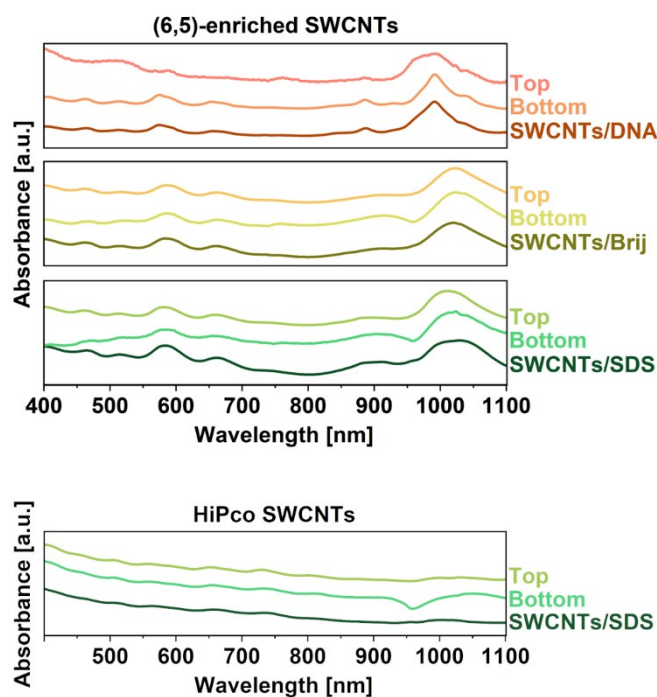


Figure S7 Absorption spectra of separated top and bottom phases, and the parent dispersion sample for SWCNTs suspended with DNA, Brij 35, and SDS surfactants. Experiments involved (6,5)-enriched CoMoCAT and HiPco SWCNTs.

SWCNTs solubilized with an anionic surfactant (sodium dodecyl sulfate, SDS), non-ionic surfactant (Brij 35), or DNA did not provide any selectivity upon addition to ATPE environment. The spectra of the top and bottom phases were very similar and matched the parent dispersions. In addition, SWCNTs dispersed by Brij and SDS exhibited poor SWCNT individualization, as the spectral peaks were not sharp. Furthermore, addition of SWCNTs dispersed with DNA was not successful, which was evident from the similarity of all three

spectra (top phase, bottom phase, parent dispersion). SDS could not also properly individualize HiPco SWCNTs, resulting in analogously unsuccessful partitioning.

DOC is known as one of the strongest surfactants for SWCNTs, promoting efficient covering²⁷ and so enhancing the stability of DOC/SWCNT dispersions. Therefore, this approach was employed to investigate interactions between PL-35 and SWCNTs, assuming that PL-35 would not be able to easily exchange DOC. Thus, all subsequent experiments were conducted with SWCNT dispersion in 2% DOC to evaluate the relationship of Pluronic and DOC towards SWCNT surface accessibility.

2.3 Selection of appropriate surfactant for SWCNT differentiation

SC and DOC were found unsuitable for purification of DOC/SWCNT dispersions as all the bottom phases resembled the spectra of parent material (Figure S8).

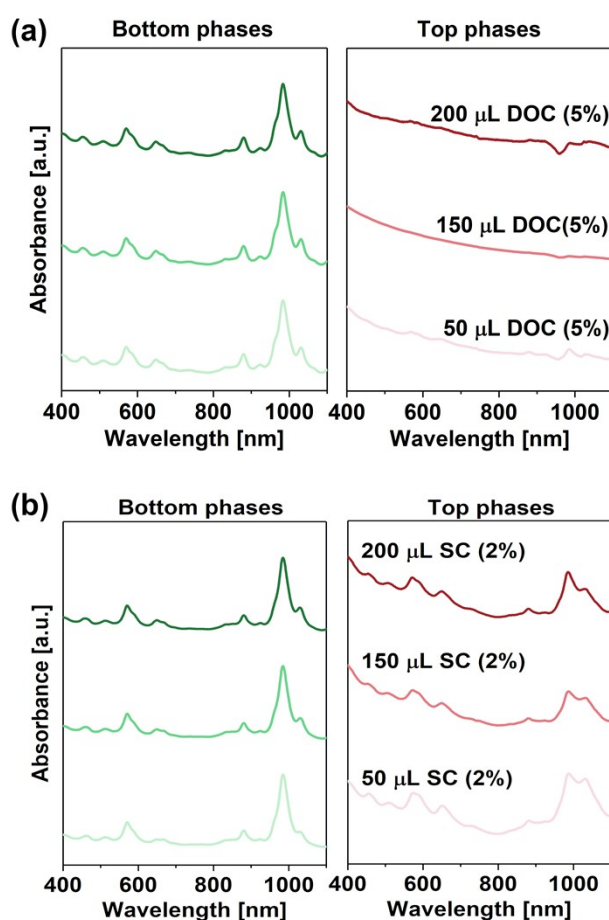


Figure S8 Effect of addition of (a) 5% DOC and (b) 2% SC solutions to control ATPE separation of SWCNTs in PL-35/DEX system. (6,5)-enriched SWCNTs were evaluated.

2.4 Analysis of purification process

2.4.1. Redistribution of SWCNTs because of addition of SDS of various concentrations

Deconvoluted spectra of bottom phase fractions collected after addition of 300 μL of SDS of 2%, 5%, 7%, and 10% concentration revealed that with increase in surfactant concentration large-diameter SWCNTs were shifted to the top phase, which increased the content of small-diameter species in the bottom phase (Figure S9).

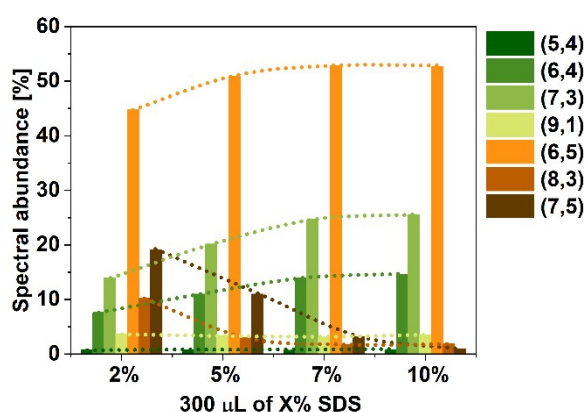


Figure S9 The influence of concentration of the added SDS solution (300 μL) on the composition of the bottom spectra. Dotted lines are to guide the eye.

2.4.2. Processing of different SWCNT raw material

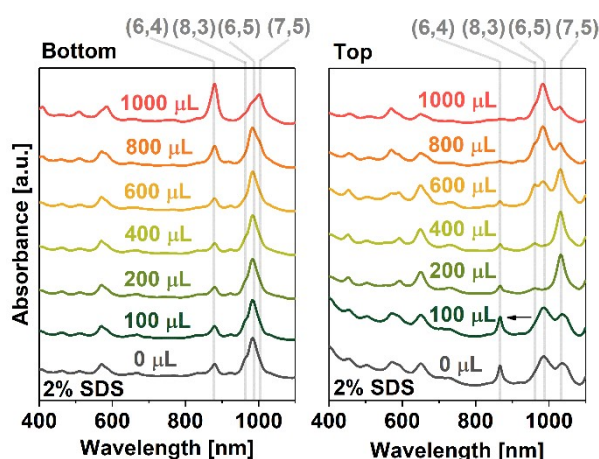


Figure S10 Effect of 2% SDS (100, 200, 400, 600, 800, and 1000 μL) as an external modulator to control ATPE separation in PL-35/DEX system, (left) the bottom and (right) top phase spectra, respectively. Unsorted HiPco SWCNTs were evaluated.

2.4.3. Application of SDBS as partitioning modulator

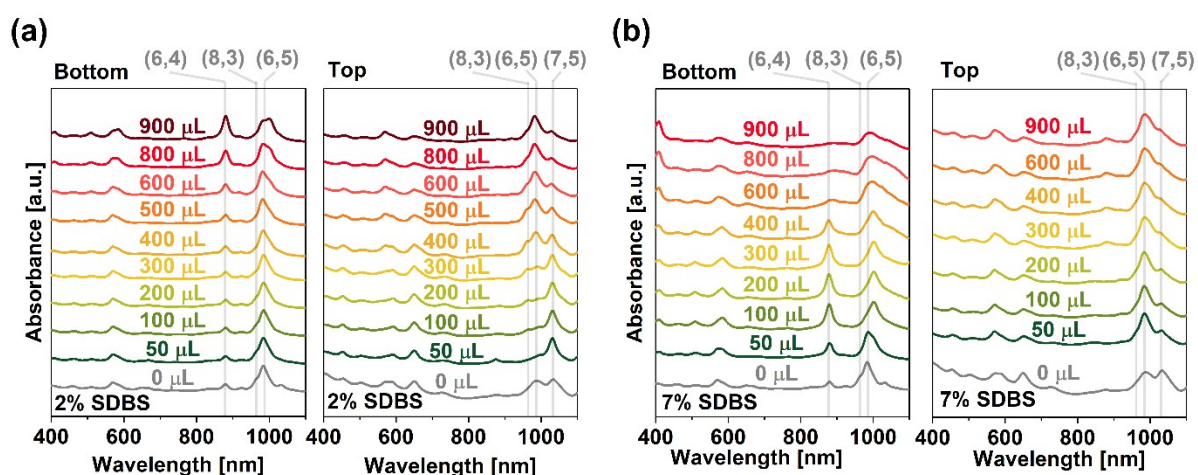


Figure S11 Effect of SDBS as an external modulator to control ATPE separation of SWCNTs in PL-35/DEX system: (a) 2% SDBS addition (50, 100, 200, 300, 400, 500, 600, 800, and 900 μL) and (b) 7% SDBS (50, 100, 200, 300, 400, 600, 800 and 900 μL) addition. (6,5)-enriched SWCNTs were evaluated.

2.4.4. Quantification of composition of isolated SWCNT fractions

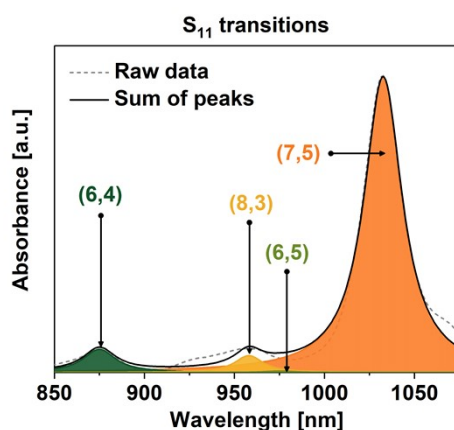


Figure S12 Example of deconvolution of peaks of individual SWCNT types (PL-35/DEX system, addition of 50 μL of 5% SDS, and (6,5)-enriched SWCNTs as feed).

2.4.5. Modeling of SWCNT-surfactant interactions

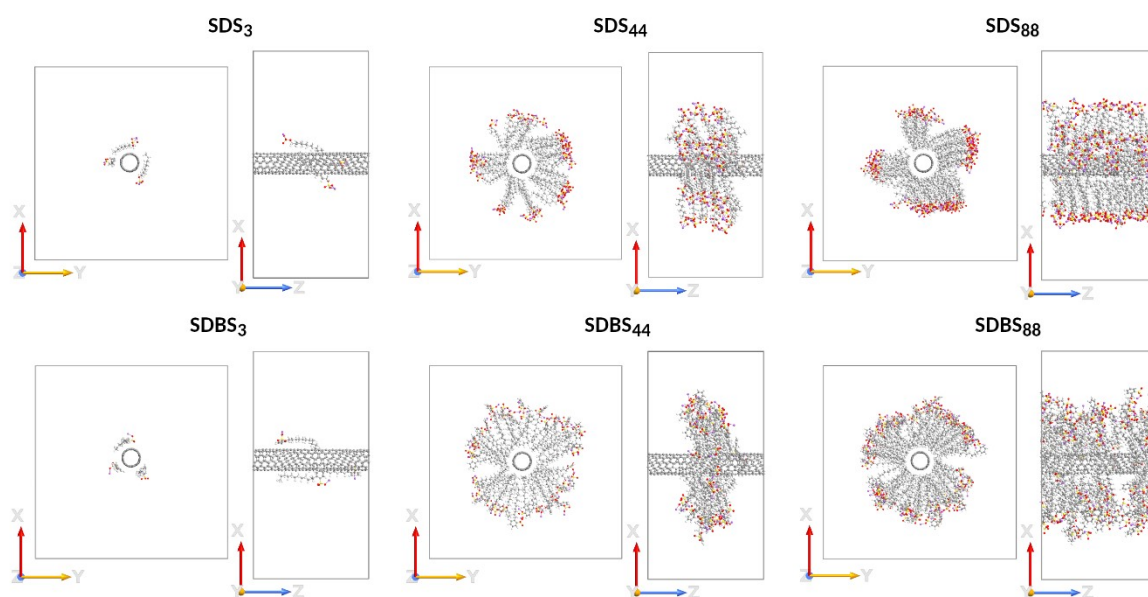


Figure S13 Snapshots of the final configurations of MC simulation box containing (6,5)-SWCNT surrounded by 3 (left), 44 (middle), and 88 (right) SDS (top) or SDBS (bottom) in a mixture of 6160 water molecules. For clarity, water molecules are excluded. C atoms are depicted in dark grey color and O, S, Na, and H are shown in red, yellow, purple, and white color, respectively.

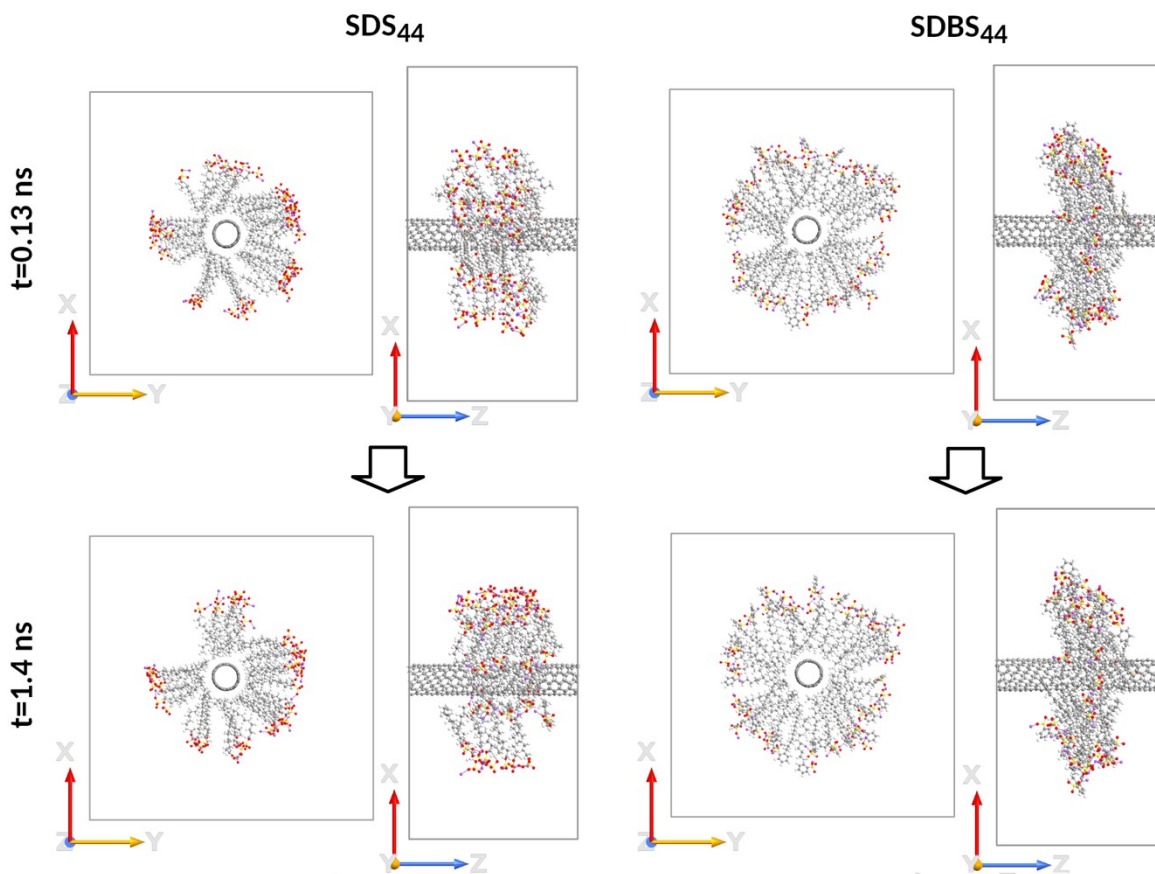


Figure S14 Snapshots of simulation box containing (6,5)-SWCNT surrounded by 44 SDS (left) or SDBS (right) in a mixture of 6160 water molecules showing the evolution of surfactant orientation toward SWCNT over time. For clarity, water molecules are excluded. C atoms are depicted in dark grey color and O, S, Na, and H are shown in red, yellow, purple, and white color, respectively. Differences in the orientation of SDS and SDBS molecules around SWCNT are still visible after extended MC simulation time.

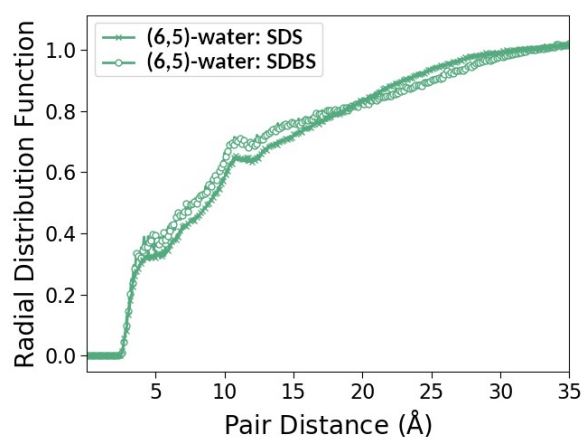


Figure S15 RDF of nanotube-water atoms for systems containing 44 SDS and 44 SDBS molecules. The magnitude of the first peak in RDF of SDBS system is higher than that of SDS system, indicating higher probability of finding water adjacent SWCNT surface in SDBS system. Hence, aggregation of SDBS molecules along Z-axis has a greater effect on SWCNT area in contact with water than the formation of bundles by SDS molecules in XY plane.

2.5 Insights into the separation mechanism

2.5.1. Change in SWCNT density upon absorption of surfactant molecules on the surface

All-atom molecular dynamics of SDS aggregates on SWCNTs carried out by Tummala et al. revealed that the SWCNT diameter was the primary factor that determined surfactant morphology and the extent to which it covered the surface. An entropic and energetic advantage was detected when SDS was deposited on SWCNTs. While, simultaneously, an enthalpic penalty was imposed as the surfactant had to bend to coat SWCNT surface²⁸.

Analogous phenomena could be used to explain the selective movement of SWCNTs from DEX to the PL-35 phase. We hypothesized that the inclusion of SDS/SDBS as an external modulator adjusted the buoyant density of various SWCNT types in ATPE system. This effect may justify the observed migration from one phase to the other depends on the amount of surfactant. Initially, when DOC-based SWCNT dispersion was introduced into the biphasic system containing surfactants, a competitive absorption process may occur on the nanotube surface between DOC and SDS/SDBS. There were three possible routes this absorption process could take place; (1) some of SDS/SDBS molecules occupied available vacant sites on the nanotube surface, (2) they replaced DOC on the nanotube surface, or, finally, (3) new surfactant molecules formed a second layer of surfactant over DOC-wrapped SWCNTs. However, either way, the effective surfactant-nanotube density changed in the presence of these species. Consequently, this environment gave rise to a certain amount of selectivity in the top and bottom phases, even at the initial stages.

3. References

1. Silva, D. F. C. *et al.* Determination of aqueous two phase system binodal curves using a microfluidic device. *Journal of Chromatography A* **1370**, 115–120 (2014).
2. Pfohl, M. *et al.* Fitting Single-Walled Carbon Nanotube Optical Spectra. *ACS Omega* **2**, 1163–1171 (2017).
3. Nair, N., Usrey, M. L., Kim, W.-J., Braatz, R. D. & Strano, M. S. Estimation of the (n,m) Concentration Distribution of Single-Walled Carbon Nanotubes from Photoabsorption Spectra. *Anal. Chem.* **78**, 7689–7696 (2006).
4. Lindau, I., Pianetta, P., Yu, K. Y. & Spicer, W. E. Photoemission of gold in the energy range 30-300 eV using synchrotron radiation. *Phys. Rev. B* **13**, 492–495 (1976).
5. Stando, G., Łukawski, D., Lisiecki, F. & Janas, D. Intrinsic hydrophilic character of carbon nanotube networks. *Applied Surface Science* **463**, 227–233 (2019).
6. Chew, H. B., Moon, M.-W., Lee, K. R. & Kim, K.-S. Compressive dynamic scission of carbon nanotubes under sonication: fracture by atomic ejection. *Proceedings of the Royal Society A: Mathematical, Physical and Engineering Sciences* **467**, 1270–1289 (2010).
7. Arrigo, R. *et al.* Sonication-Induced Modification of Carbon Nanotubes: Effect on the Rheological and Thermo-Oxidative Behaviour of Polymer-Based Nanocomposites. *Materials* **11**, 383 (2018).
8. Shea, M. J., Wang, J., Flach, J. T., Zanni, M. T. & Arnold, M. S. Less severe processing improves carbon nanotube photovoltaic performance. *APL Materials* **6**, 056104 (2018).
9. Rappe, A. K., Casewit, C. J., Colwell, K. S., Goddard, W. A. I. & Skiff, W. M. UFF, a full periodic table force field for molecular mechanics and molecular dynamics simulations. *J. Am. Chem. Soc.* **114**, 10024–10035 (1992).
10. Schneider, J. *et al.* ATK-ForceField: a new generation molecular dynamics software package. *Modelling Simul. Mater. Sci. Eng.* **25**, 085007 (2017).

11. Synopsis QuantumATK version 2022.03-SP1,
<https://www.synopsys.com/silicon/quantumatk.html> (accessed 10-09-2022).
12. Essmann, U. *et al.* A smooth particle mesh Ewald method. *J. Chem. Phys.* **103**, 8577–8593 (1995).
13. Rappe, A. K. & Goddard, W. A. I. Charge equilibration for molecular dynamics simulations. *J. Phys. Chem.* **95**, 3358–3363 (1991).
14. Jones, J. E. & Chapman, S. On the determination of molecular fields.—I. From the variation of the viscosity of a gas with temperature. *Proceedings of the Royal Society of London. Series A, Containing Papers of a Mathematical and Physical Character* **106**, 441–462 (1924).
15. Jones, J. E. & Chapman, S. On the determination of molecular fields. —II. From the equation of state of a gas. *Proceedings of the Royal Society of London. Series A, Containing Papers of a Mathematical and Physical Character* **106**, 463–477 (1924).
16. Lennard-Jones, J. E. Cohesion. *Proc. Phys. Soc.* **43**, 461 (1931).
17. Martínez, L., Andrade, R., Birgin, E. G. & Martínez, J. M. PACKMOL: A package for building initial configurations for molecular dynamics simulations. *Journal of Computational Chemistry* **30**, 2157–2164 (2009).
18. Liu, D. C. & Nocedal, J. On the limited memory BFGS method for large scale optimization. *Mathematical Programming* **45**, 503–528 (1989).
19. Berendsen, H. J. C., Postma, J. P. M., van Gunsteren, W. F., DiNola, A. & Haak, J. R. Molecular dynamics with coupling to an external bath. *J. Chem. Phys.* **81**, 3684–3690 (1984).
20. Martyna, G. J., Klein, M. L. & Tuckerman, M. Nosé–Hoover chains: The canonical ensemble via continuous dynamics. *J. Chem. Phys.* **97**, 2635–2643 (1992).

21. Bal, K. M. & Neyts, E. C. On the time scale associated with Monte Carlo simulations. *J. Chem. Phys.* **141**, 204104 (2014).
22. Neyts, E. C. & Bogaerts, A. Combining molecular dynamics with Monte Carlo simulations: implementations and applications. *Theor Chem Acc* **132**, 1320 (2012).
23. Fagan, J. A. Aqueous two-polymer phase extraction of single-wall carbon nanotubes using surfactants. *Nanoscale Adv.* **1**, 3307–3324 (2019).
24. Pereira, J. F. B., Freire, M. G. & Coutinho, J. A. P. Aqueous two-phase systems: Towards novel and more disruptive applications. *Fluid Phase Equilibria* **505**, 112341 (2020).
25. Podlesny, B., Shiraki, T. & Janas, D. One-step sorting of single-walled carbon nanotubes using aqueous two-phase extraction in the presence of basic salts. *Scientific Reports* **10**, 9250 (2020).
26. Lyu, M., Meany, B., Yang, J., Li, Y. & Zheng, M. Toward Complete Resolution of DNA/Carbon Nanotube Hybrids by Aqueous Two-Phase Systems. *J. Am. Chem. Soc.* **141**, 20177–20186 (2019).
27. Lin, C.-W. *et al.* Creating fluorescent quantum defects in carbon nanotubes using hypochlorite and light. *Nat Commun* **10**, 2874 (2019).
28. Tummala, N. R. & Striolo, A. SDS Surfactants on Carbon Nanotubes: Aggregate Morphology. *ACS Nano* **3**, 595–602 (2009).